Click Here for Full Article

Anomalous early aftershock decay rate of the 2004 Mw6.0 Parkfield, California, earthquake

Zhigang Peng,[1,2] John E. Vidale,[1] and Heidi Houston[1]

Received 28 April 2006; revised 26 June 2006; accepted 25 July 2006; published 7 September 2006.

[1] We analyze the seismicity rate immediately after the 2004 Mw6.0 Parkfield, California, earthquake from near-source seismograms. By scrutinizing high-frequency signals, we can distinguish mainshock coda from early aftershocks occurring as soon as 30 s after the mainshock. We find, as expected, that a significant fraction of aftershocks in the first few hours after the main shock are missing in the Northern California Seismic Network catalog. We observe a steady rate of aftershocks in the first 130 s, followed by a power-law decay of aftershock activity. Thus, there appears to be a distinct early stage of aftershock activity that does not fit the Omori's law with a constant p value, a phenomenon that we refer to as *Early Aftershock Deficiency* (EAD). Our observation suggests that mainshock rupture and aftershocks are distinct processes, not described by a single Omori's law. Several physical models of aftershocks can explain the EAD. **Citation:** Peng, Z., J. E. Vidale, and H. Houston (2006), Anomalous early aftershock decay rate of the 2004 Mw6.0 Parkfield, California, earthquake, *Geophys. Res. Lett.*, *33*, L17307, doi:10.1029/2006GL026744.

1. Introduction

[2] A large shallow earthquake is typically followed by aftershocks that diminish in rate approximately as the inverse of the elapsed time since the mainshock, a phenomenon known as the Omori's law [*Omori*, 1894]. Later, *Utsu et al.* [1995] introduced the modified Omori's law,

$$R(t) = \frac{K}{(t+c)^p}, \tag{1}$$

where K is the aftershock productivity, p is the exponent that is generally close to 1, and c is a constant time shift. The c value is introduced to eliminate the singularity in the aftershock rate as t goes to zero.

[3] The existence of the c value and its physical meaning are still under debate [*Utsu et al.*, 1995], most likely because it is difficult to observe early aftershock activity in the noisy aftermath of large earthquakes [*Kagan*, 2004]. Yet this period marks the transition from mainshock to aftershocks, and holds valuable information about the underlying mechanisms that control the aftershock occurrence [e.g., *Nur and Booker*, 1972; *Das and Scholz*, 1981; *Dieterich*, 1994; *Ben-Zion and Lyakhovsky*, 2006].

[4] Previous studies on aftershock decay rate mainly used earthquakes in existing catalogs [*Utsu et al.*, 1995]. However, they are known to be incomplete immediately after large mainshocks, mainly due to overlapping of the codas of large aftershocks and overload of processing facilities [*Kagan*, 2004]. Several recent studies have focused on the high-frequency radiation of earthquakes, and obtained useful information about the mainshock rupture and the aftershocks [e.g., *Ishii et al.*, 2005; Z. Peng et al., Anomalous seismicity rates immediately before and after main shock rupture from high-frequency waveforms in Japan, submitted to *Journal of Geophysical Research*, 2006].

[5] Here, we systematically analyze the early aftershock decay rate of the 2004 Mw6.0 Parkfield, California, earthquake [*Bakun et al.*, 2005] by scrutinizing high-frequency signals from seismograms recorded near the source region. The mainshock ruptured the Parkfield section of the San Andreas fault (SAF) (Figure 1). Many near-field, unclipped and continuous seismograms for the mainshock and its aftershocks were recorded.

2. Data and Analysis Procedure

[6] We use waveforms recorded by the surface station PKD of the Berkeley Digital Seismic Network, 13 borehole stations at the High Resolution Seismic Network (HRSN), and the San Andreas Fault Observatory at Depth Pilot Hole (SAFOD_PH) array. The sampling frequencies are 80 Hz, 250 Hz, and 500 Hz, for station PKD, HRSN array, and SAFOD_PH array, respectively.

[7] Since seismic codas of the mainshock have little high frequency content, we apply a two-pass Butterworth high-pass filter to detect early aftershocks buried inside the mainshock coda. The corner frequencies of the high-pass filter are 20 Hz, 40 Hz, and 60 Hz for waveforms recorded by station PKD, HRSN array, and SAFOD_PH array, respectively. The choice of the corner frequencies represents a compromise between the sampling frequency and signal-to-noise ratio. The results are similar for a range of high-pass filters, but the data filtered with higher frequency have sharper onsets and coda that decay more rapidly.

[8] Next, we compute the envelopes of the high-pass-filtered seismograms, stack envelopes for the three components, take the logarithm, and smooth the resulting envelope by a moving median operator with a half-width of 10 data points (Figure 2). We stack the three-component data to enhance the signal, and to produce P and S double arrivals for event identification. We then shift in amplitude each envelope using the average values within 1000 s (within 50 s for envelope of the SAFOD_PH array, as limited by the

[1]Department of Earth and Space Sciences, University of California, Los Angeles, California, USA.
[2]Now at School of Earth and Atmospheric Sciences, Georgia Institute of Technology, Atlanta, Georgia, USA.

Copyright 2006 by the American Geophysical Union.
0094-8276/06/2006GL026744$05.00

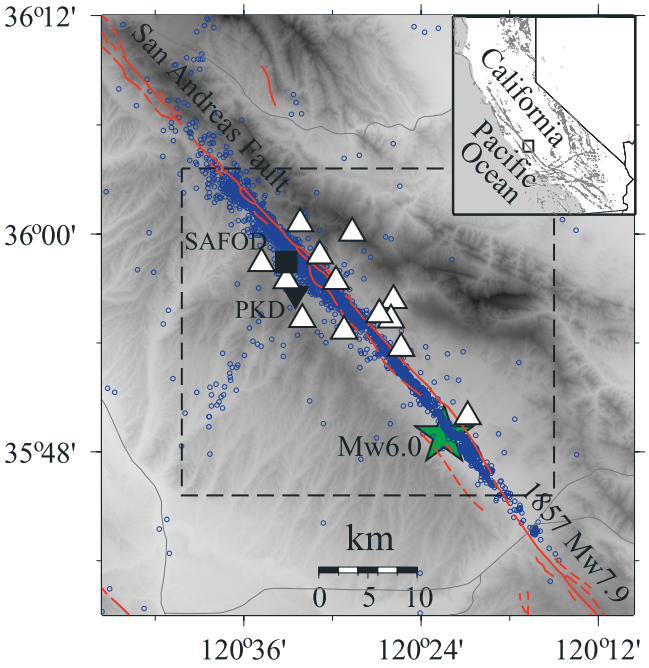

Figure 1. Map of the study area, including the epicentral location of the 2004 Mw6.0 Parkfield earthquake (green star), and aftershocks listed in the Northern California Seismic Network (NCSN) catalog (blue dots). The inverted solid triangle denotes station PKD of the Berkeley Digital Seismic Network. Open triangles represent 13 stations in the High Resolution Seismic Network (HRSN). The SAFOD pilot hole array is marked by the solid square. Shaded background indicates topography with light shades denoting lower elevation and darker shades indicating higher elevation. The red and gray lines denote the surface traces of the San Andreas fault, and the nearby highways, respectively. The label "1857 M7.9" indicates the northern extent of the rupture zone of the 1857 Fort Tejon earthquake. The dashed line defines the aftershock region of the Parkfield mainshock. The inset illustrates the tectonic environment in California with the box corresponding to our study area.

available data) before the mainshock so that the noise level before the main shock for each shifted envelope has an average value of zero.

3. Results

3.1. Aftershock Comparison

[9] Next, we compare aftershocks of the Parkfield mainshock identified from the envelope for station PKD and those listed in the NCSN catalog (Figure 2c). The aftershocks are selected from the catalog within a box (latitude: 35.76° to 36.06°; longitude: −120.67° to −120.25°) with no depth restriction. The box is suggested by the NCEDC website for data related to the 2004 Parkfield earthquake (http://www.ncedc.org/2004parkfield.html). We manually identify aftershocks by searching for clear double peaks in the envelope that correspond to the *P* and *S* arrivals of each event. A total of 46 events within 300 s after the mainshock are identified by our handpicking procedure. In comparison, only two aftershocks (and the mainshock itself) are listed in the NCSN catalog in this time period (Figure 2b). A total of 72 events are listed in the NCSN catalog within the first hour after the mainshock. In comparison, our method identified 247 events from the envelope for the surface station PKD during the same period.

[10] Since the aftershocks of the Parkfield mainshock span about 35 km along the SAF [*Bakun et al.*, 2005], it is difficult to assign magnitudes to aftershocks identified from waveforms at only one or a few nearby stations. Without a common magnitude calibration and threshold magnitude, a direct comparison of the number of events listed in the NCSN catalog and identified from the high-pass-filtered envelope is not feasible.

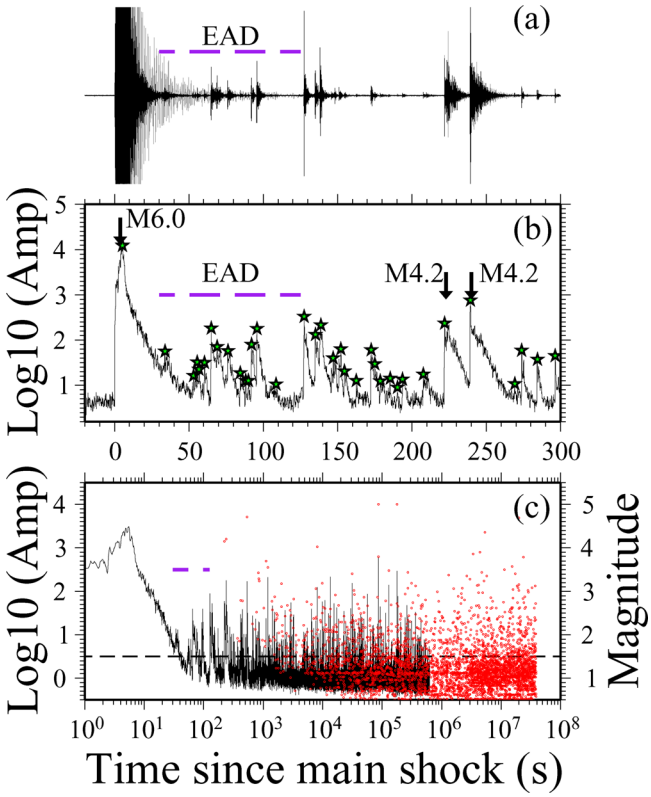

Figure 2. (a) Original (gray line) and high-pass-filtered (dark line) vertical-component seismogram recorded by station PKD. The trace is clipped, with the peak amplitude of the mainshock off-scale. (b) Logarithm of the envelope (dark line) generated by stacking the envelopes of the high-pass-filtered three-component seismograms for station PKD. Each blue star marks an event identified by our handpicking procedure. The vertical arrows mark the two events listed in the NCSN catalog within 300 s after the mainshock (and the mainshock itself). The dashed purple line mark the time period of [30–132] s, when *Early Aftershock Deficiency* (EAD) is observed. (c) Comparison between the envelope for station PKD (gray line) and aftershocks (small red dots) listed in the NCSN catalog in logarithmic time scale. The envelope level has been shifted so that the pre-event noise level is zero. The horizontal dashed line marked the cutoff amplitude of 0.5 (in logarithmic scale) above which the amplitudes are summed to obtain the seismicity rate in Figure 4.

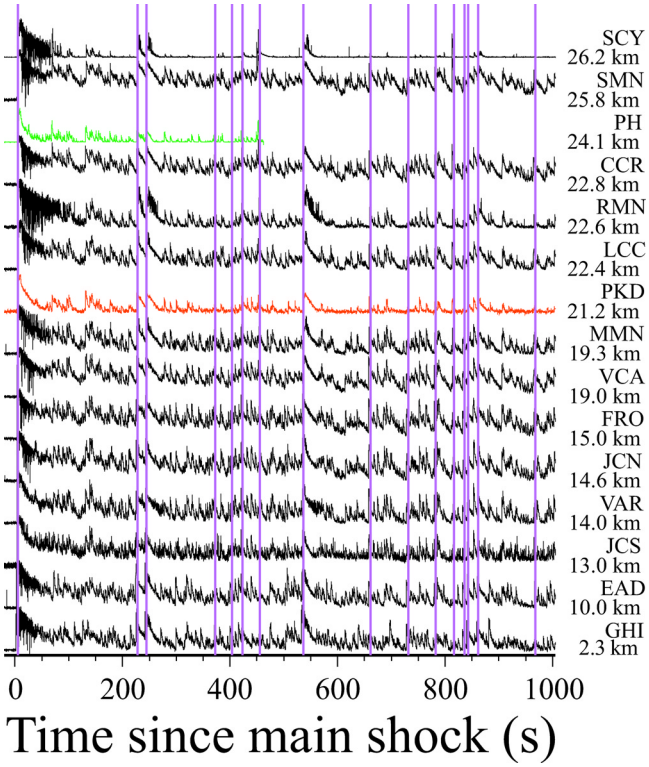

Figure 3. Envelopes for 13 HRSN borehole stations (solid line), station PKD (red line), and SAFOD PH station S26 (green line) ordered from bottom to top according to the hypocentral distances, which are listed on the right side. The vertical lines mark the occurrence time of the mainshock, and the 15 aftershocks listed in the NCSN catalog within 1000 s after the mainshock. Clearly, many more small aftershocks occurred than were in the NCSN catalog.

3.2. Direct Estimation of Seismicity Rate From Envelope

[11] The resulting envelopes are very similar for stations at different epicentral distances (Figure 3). This indicates that the high-frequency signals are coherent among the stations we analyzed, and are indicative of the level of seismic activity near the source region. So we directly estimate the seismicity rate immediately after the Parkfield mainshock from each envelope (Figure 3). In detail, we linearly sum the envelope value where it is ≥ 0.5 (roughly corresponding to a nominal signal-to-noise ratio of 3) for each time window. The time windows are fixed to a width of 0.2 in log time (s). We then slide the time window by 0.01 in log time (s), and then divide the resulting amplitude summation by the length of the time window (in linear time) to obtain the seismicity rate for each station after the mainshock (Figure 4). The cutoff amplitude level of 0.5 is justified by noting that fluctuations in amplitude above 0.5 are highly correlated and directly related to aftershock activity, while fluctuations below 0.5 (near zero noise level) often are not. The choice of time window with width of 0.2 in log time second represents a compromise between a need to have long enough time window for a smooth curve of seismicity rate, but short enough to show the variation. A similar technique was used to estimate the difference in seismic activity in Japan before and after the passage of the seismic waves generated by the 2003 Mw8.1 Tokachi-oki earthquake [*Miyazawa and Mori*, 2005].

[12] Next, we compare the seismicity rates from envelopes for station PKD, the logarithmic average of 11 out of 13 HRSN stations, and the logarithmic average of 7 stations of the SAFOD_PH array (Figure 4). Envelopes for stations JCN and SCY of the HRSN are not used due to high pre-event noise level and short seismic records. To obtain a similar baseline for comparison of seismicity rates at different stations, we normalize them to the same value of 1 at 100 s after the mainshock. We also compute the seismicity rates for both pre-mainshock seismicity and aftershocks from the NCSN catalog ($m \geq 1.5$). We then shift the obtained seismicity rates so that the aftershock rate from the NCSN catalog and the envelope at station PKD match at 10^6 s. Although the rate inferred from the envelope fluctuates more than that from the catalog, the seismicity rates estimated from different methods are similar.

[13] Since the NCSN catalog is not complete to $m \geq 1.5$ in the first hour or so after the mainshock (Figure 2c), we fit the aftershock rate for NCSN catalog after 3600 s (1 hour) by a least-squares fit using the Omori's law ($r(t) \sim 1/t^p$). The p value obtained is 0.86 ± 0.03. The error is the 95% confidence interval based on a bootstrap analysis (1000 resamplings of the set of aftershocks). In comparison, the p value for seismicity rate at station PKD is 0.69 ± 0.03

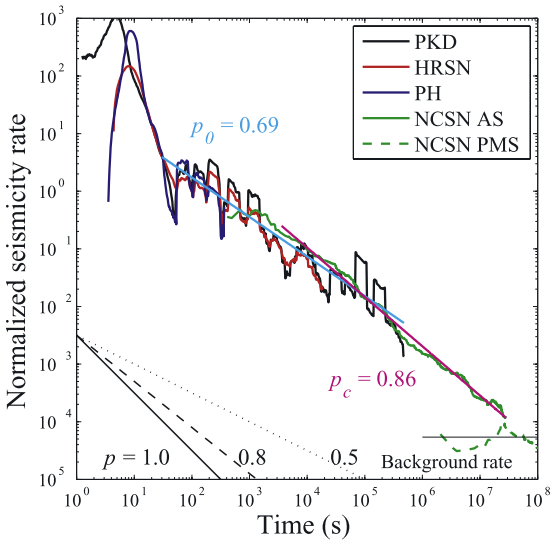

Figure 4. Aftershock seismicity rates as a function of the time since the mainshock obtained from the high-pass-filtered envelopes for station PKD (dark line), HRSN array (red line), SAFOD Pilot Hole array (blue line), and from the NCSN catalog with $m \geq 1.5$ (green line). The green dashed line shows the pre-mainshock seismicity rate over the time interval of $[10^7 - 10^8]$ s ([115.7–1157] days) before the mainshock. This gives an average background seismicity rate of 5.4×10^{-5}, which is indicated by the horizontal dark line. The cyan and magenta lines denote least-squares fitting for the seismicity rate observed at station PKD in the time interval of $[30 - 6.3 \times 10^5]$ s, and from the NCSN aftershocks in the time interval of $[3600 - 2.9 \times 10^7]$ s. The obtained p values are listed. The solid, dashed and dotted lines show the reference rates with $p = 1.0$, 0.8, and 0.5.

between 30 s and 6.3×10^5 s (~7.3 days). The seismicity rate within 30 s is dominated by the mainshock coda, and hence is excluded from the time interval chosen for fitting.

3.3. Statistical Method to Find Break of Slope in the Seismicity Rate

[14] We note that the seismicity rate in the first few hundred seconds is approximately steady, instead of following the same decay rate as at later times (Figure 4). To quantify the statistical significance of such a break of slope in the seismicity rate, we apply the Bayesian Information Criterion (BIC) [*Leonard and Hsu*, 1999; *Main et al.*, 1999],

$$BIC = L(y) - \frac{1}{2} m \ln(n/2\pi), \quad (2)$$

where $L(y)$ is the maximum likelihood estimate of the model, m is the number of unknown parameters, and n is the sample size.

[15] For a single-slope model, the unknown parameters are intercept, slope and variance. For a double-slope model, there are 5 unknown parameters: intercept, two slopes, break point and variance [*Main et al.*, 1999]. The peak of the BIC values for the double-slope model is higher than that for the single-slope model (Figure 5), indicating that the break of slope in the seismicity rate is statistically significant.

[16] The break point $t^* = 132$ s is found when the BIC reaches its maximum value. The best fitting p values are -0.18 ± 0.20 between 30 and 132 s, and 0.74 ± 0.03 between 132 and 10^6 s. A negative p value immediately after the mainshock indicates that the aftershock activity may actually increase with time in the first 132 s, as was suggested by the lack of large aftershocks in Figure 2c. However, the 95% confidence interval is very large, due to large fluctuations in the seismic activity and a relatively short time interval. So we cannot rule out the possibility that the early aftershock rate may decay with a small positive p value. However, it is clear that the aftershock activity is decaying more slowly in the first ~130 s than at later time intervals. The average envelope of the HRSN data also shows a nearly flat rate similar to that of station PKD from 30 to 132 s (Figure 4).

4. Interpretation

[17] By scrutinizing the high-frequency signals, we were able to distinguish mainshock coda from aftershocks occurring as early as 30 s after the mainshock. We found that a significant fraction of aftershocks in the first few hours after the Parkfield mainshock is missing from the NCSN catalog. This indicates that the commonly observed c values (on the order of a few hours or more) [e.g., *Shcherbakov and Turcotte*, 2006] are most likely caused by missing aftershocks in the catalog.

[18] However, the newly-detected early aftershocks are fewer than predicted by extrapolation of the aftershock rate from 10^7 s back in time to ~100 s according to the Omori's law. In particular, we observe a fairly steady rate of aftershocks in the first ~130 s, followed by a power-law decay of activity with time afterward. Thus, there appears to be a distinct early stage of low aftershock activity that marks a transition from mainshock rupture to numerous aftershocks, which we refer to as *Early Aftershock Deficiency* (EAD).

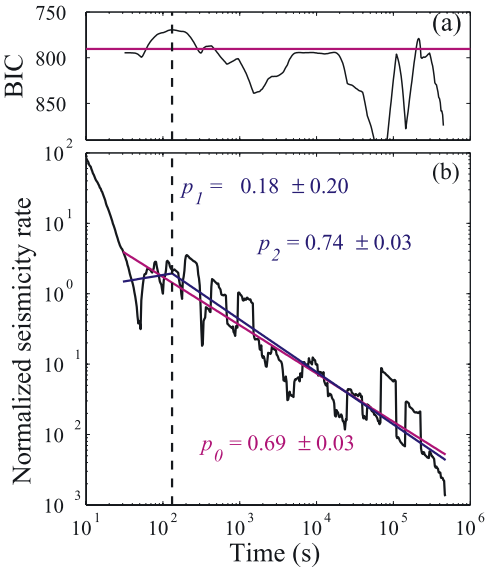

Figure 5. (a) The Bayesian Information Criterion (BIC) plotted as a function of the change point t^* for a double-slope model (dark line), compared with a single-slope model (magenta line) for seismicity rate at station PKD. The dashed vertical line marks the location of the best fitting break of slope. (b) Seismicity rate as a function of the time since the mainshock obtained from the high-pass-filtered envelopes for station PKD. The best fitting lines using the single-slope model (magenta line) and the double-slope model (blue line) are shown. The obtained p values are listed.

[19] Our observation indicates that the seismicity rate does not increase towards infinity as the time goes to 0, as implied by the original Omori's law. This result argues against a model in which mainshock rupture propagation is represented as no more than the superposition of aftershocks [*Kagan*, 2004], and suggests that a mainshock rupture and its aftershock sequence are distinct processes, not described by a single Omori's law. This notion is also implied by the results of *Kagan and Houston* [2005], who noted a factor of 30 disparity between the level of aftershock activity and the level of peak mainshock moment release. The disparity likely reflects the difference in the dynamic and static stresses that control the mainshock rupture and the aftershock processes. The mainshock rupture is highly organized in space and time, and controlled mainly by propagating seismic stress waves. In comparison, the aftershock process, which spans a much greater temporal extent and lacks such systematic space-time migration, is likely to be controlled by static stresses, or residual effects from the past dynamic stresses.

[20] Our observation of a near-constant seismicity rate immediately after the mainshock may be consistent with the predictions of several physical models for aftershock processes, including the rate- and state-dependent friction model [e.g., *Dieterich*, 1994], the stress corrosion model [e.g., *Main*, 1999; *Gomberg*, 2001], and the damage rheology model [*Ben-Zion and Lyakhovsky*, 2006]. We note that

additional information, such as long-term seismicity rate, thermal gradient, loading rate, and seismic coupling, is needed to distinguish between these models.

5. Conclusion

[21] We analyzed the seismicity rate immediately after the 2004 Parkfield mainshock from high-frequency continuous waveforms. We found that a significant fraction of aftershocks were not in the NCSN catalog in the first few hours after the mainshock. However, the newly detected events are not numerous enough to match the aftershock rate extrapolated from later times. We observed a fairly steady rate of aftershocks in the first ~130 s, followed by the Omori power-law decay of activity. The observation may be consistent with several physical models of aftershock processes. Our result indicates that a mainshock rupture and its aftershock activity are distinct processes, separated by an interval of Early Aftershock Deficiency (EAD), and thus not described by a single Omori's law.

[22] **Acknowledgments.** We thank Northern California Earthquake Data Center for making the catalog and waveforms of the 2004 Parkfield earthquake available. Yehuda Ben-Zion, Emily Brodsky, Paul Davis, Debi Kilb, Yan Kagan, and an anonymous reviewer generously provided commentary. This research was supported by the Southern California Earthquake Center. SCEC is funded by NSF Cooperative Agreement EAR-0106924 and USGS Cooperative Agreement 02HQAG0008. The SCEC contribution number for this paper is 1028.

References

Bakun, W. H., et al. (2005), Implications for prediction and hazard assessment from the 2004 Parkfield earthquake, *Nature*, *437*, 969–974, doi:10.1038/nature04067.

Ben-Zion, Y., and V. Lyakhovsky (2006), Analysis of aftershocks in a lithospheric model with seismogenic zone governed by damage rheology, *Geophys. J. Int.*, *165*, 197–210.

Das, S., and C. Scholz (1981), Off-fault aftershock clusters caused by shear stress increase?, *Bull. Seismol. Soc. Am.*, *71*, 1669–1675.

Dieterich, J. (1994), A constitutive law for rate of earthquake production and its application to earthquake clustering, *J. Geophys. Res.*, *99*, 2601–2618.

Gomberg, J. (2001), The failure of earthquake failure models, *J. Geophys. Res.*, *106*, 16,253–16,264.

Ishii, M., P. M. Shearer, H. Houston, and J. E. Vidale (2005), Rupture extent, duration, and speed of the 2004 Sumatra-Andaman earthquake imaged by the Hi-Net array, *Nature*, *435*, 933–936, doi:10.1038/nature03675.

Kagan, Y. Y. (2004), Short-term properties of earthquake catalogs and models of earthquake source, *Bull. Seismol. Soc. Am.*, *94*, 1207–1228.

Kagan, Y. Y., and H. Houston (2005), Relation between mainshock rupture process and Omori's law for aftershock moment release rate, *Geophys. J. Int.*, *163*, 1039–1048.

Leonard, T., and J. S. J. Hsu (1999), *Bayesian Methods*, Cambridge Univ. Press, New York.

Main, I. G. (1999), Applicability of time-to-failure analysis to accelerated strain before earthquakes and volcanic eruptions, *Geophys. J. Int.*, *139*, F1–F6.

Main, I. G., T. Leonard, O. Papasouliotis, C. G. Hatton, and P. G. Meredith (1999), One slope or two? Detecting statistically-significant breaks of slope in geophysical data, with application to fracture scaling relationships, *Geophys. Res. Lett.*, *26*, 2801–2804.

Miyazawa, M., and J. Mori (2005), Detection of triggered deep low-frequency events from the 2003 Tokachi-oki earthquake, *Geophys. Res. Lett.*, *32*, L10307, doi:10.1029/2005GL022539.

Nur, A., and J. R. Booker (1972), Aftershocks caused by pore fluid flow?, *Science*, *175*, 885–888.

Omori, F. (1894), On the aftershocks of earthquakes, *J. Coll. Sci. Imp. Univ. Tokyo*, *7*, 111–200.

Shcherbakov, R., and D. L. Turcotte (2006), Scaling properties of the Parkfield aftershock sequence, *Bull. Seismol. Soc. Am.*, in press.

Utsu, T., Y. Ogata, and R. S. Matsu'ura (1995), The centenary of the Omori formula for a decay law of aftershock activity, *J. Phys. Earth*, *43*(1), 1–33.

H. Houston and J. E. Vidale, Department of Earth and Space Sciences, University of California, 595 Charles Young Drive East, Los Angeles, CA 90095-1567, USA.

Z. Peng, School of Earth and Atmospheric Sciences, 311 Ferst Drive, Georgia Institute of Technology, Atlanta, GA 30332, USA. (zhigang.peng@eas.gatech.edu)